Pol. J. Environ. Stud. Vol. 33, No. 1 (2024), 455-466
DOI: *10.15244/pjoes/170824* ONLINE PUBLICATION DATE: 2023-11-07

Original Research

Deformation Characteristics of Fiber-Reinforced Cured Lightweight Soils under Dry and Wet Cycles and Intermittent Loading

Aiwu Yang*, Binbin Wang

College of Environmental Science and Engineering, Donghua University, Shanghai, China

Received: 4 July2023
Accepted: 8 August 2023

Abstract

In practical engineering applications, cured lightweight soils are commonly used as roadbed fillers and subjected to intermittent and discontinuous traffic loads. However, previous studies primarily focused on the effects of continuous loading on the mechanical properties of cured soils. To address this knowledge gap, this study investigated the deformation characteristics of fiber-reinforced cured lightweight soils under dry and wet cycles and intermittent loading. Dynamic triaxial tests with varying intermittent ratios and numbers of dry and wet cycles were conducted to assess the influence of these factors on the accumulated plastic strain of fiber-reinforced cured lightweight soils. Based on the test results, a prediction model was developed to estimate the accumulated plastic strain of the cured soils under intermittent loading. The findings indicated that the interval length has a dampening effect on the accumulated plastic deformation of the soil, thereby improving its ability to resist deformation. Additionally, the accumulation of plastic deformation gradually increased with the number of wet and dry cycles but eventually stabilized. In multistage loading, the accumulated plastic strain displayed a rapid increase and stabilization trend similar to that in observed the first loading stage. However, the magnitude of the cyclic dynamic stress ratio determines the deformation at later loading stages. Finally, an improved exponential model was used to establish and validate a prediction model for the cumulative plastic strain of the fiber-reinforced cured lightweight soil under intermittent loading (single and multistage). This prediction model provides important guidance for the practical application of fiber-reinforced cured lightweight soils in engineering projects.

Keywords: fiber-reinforced cured lightweight soil, dry and wet cycles, intermittent loading, cumulative plastic deformation

*e-mail: wayyjk@dhu.edu.cn

Introduction

Dredged subsoil is a type of municipal waste in the form of sludge that consists of clay, silt, organic matter, and various mineral components. It is characterized by high water content, low strength, high heavy-metal content, complex composition, and an undesirable odor. In recent years, China has generated more than 10×10^9 m^3 of dredged soil annually, leading to significant environmental and safety issues related to its storage. Consequently, finding alternative sludge treatments and methods to reduce subsoil pollution through reuse has become a major concern for researchers. Some studies have found that the use of curing technology to convert dredged soil into fiber-reinforced cured lightweight soil and its application in roadbed engineering can effectively prevent secondary contamination of the subsoil and reduce treatment costs [1-4].

The mechanical properties of roadbed fillers are influenced by climate and traffic loads. Most areas in southern China experience a subtropical monsoon climate characterized by high temperatures and rainfall in summer, and low temperatures and rainfall in winter. Roadbed soils are inevitably subjected to wet-dry cycles, resulting in significant changes in their mechanical properties [5-8]. Additionally, the roadbed is subjected to dynamic vehicular loads [9-11]. The combined effects of the wet and dry cycles and cyclic dynamic loading on the deformation and strength of the cured soil are not negligible. However, most studies have focused on clay and expansive soils. For example, Long et al. studied the deformation characteristics of red clay soils under dry and wet conditions and dynamic loading and found that the dynamic stress-strain curves were nonlinear and exhibited strong hardening behavior [12]. Liu and Chen discovered that the dynamic strength of soil decreased with an increase in the number of wet and dry cycles and eventually stabilized after a certain threshold [13, 14]. Chen developed a predictive model for dynamic strain developing in powdered clay under dry, wet, and dynamic loads [15]. Wang investigated the effects of dry and wet cyclic actions on the dynamic strength of compacted loess through dynamic triaxial and electron microscopy scanning tests, revealing the deterioration mechanism [16]. Zhong found that dry and wet cyclic actions led to a decrease in the critical dynamic stress and an increase in the dynamic residual deformation of fly ash-amended loess [17].

These studies used continuous loading to simulate the effect of dynamic vehicular loading on roadbeds. However, in practical engineering, dynamic loading is not continuous. For instance, the foundation soil is not subjected to train loads during certain time intervals of subway operations, such as during train stoppages or overnight periods. Similarly, intermittent periods exist for the vehicle loads borne by roads. Therefore, in dynamic testing, the effects of intermittent loading on the soil must be considered. Current research on the dynamic properties of cured soils under intermittent loading is relatively limited, and only single-stage loading with constant dynamic stress has been considered. Fujiwara, Zheng, and Nie used single-stage loading to investigate the effects of intermittent loading on pore pressure and accumulated plastic deformation in soft clay soil. Studies on cumulative plastic deformation of cured soils under dry, wet, and intermittent loading conditions are limited [18-21]. Therefore, it is essential to study the deformation characteristics of cured soils under the combined effects of wet and dry cycles and intermittent dynamic loading.

To address this research gap, this study considers the effects of dry and wet cycling and intermittent load superposition on fiber-reinforced cured lightweight soils. Dynamic triaxial tests with intermittent loading (both single-stage and multi-stage) were conducted to analyze the effects of different numbers of dry-wet cycles, intermittent ratios, and multi-stage dynamic stress levels on the cumulative plastic deformation of fiber-reinforced cured lightweight soils. Additionally, the classical exponential model for predicting the cumulative plastic deformation was improved, thereby enabling the enhanced model to predict the development of cumulative plastic strain in intermittently loaded cured soils. These findings provide valuable insights into the practical application of fiber-reinforced cured lightweight soils in engineering projects.

Materials and Test Methods

Materials

The test sample used for this study was bottom mud collected from a river and lake that had been dredged by a dredging center in Shanghai. The mud was in the form of black lumps, as illustrated in Fig. 1. The fundamental physical properties of the river and lake substrates are listed in Table 1. The substrate was dried in an oven, ground using a grinder to remove large particles and impurities, and sieved. The sieved substrates were then sealed and stored.

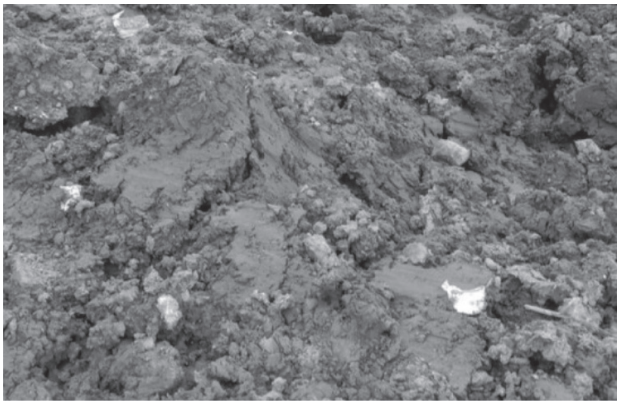

Fig. 1. Sample photograph of the soil at the banks of the river and lake dredged by a dredging center in Shanghai.

Table 1. Basic physical properties of river and lake substrates.

Water content ω/%	Density ρ/(g·cm^{-3})	Specific gravity G_s	Organic matter content /%
57.2	1.26	1.6	5.38

To create fiber-reinforced cured lightweight soils, cement, and quicklime were used as curing materials. Basalt fiber is an inorganic silicate fiber with natural compatibility with silicate materials (cement, cobalt fiber is an inorganic silicate fiber with natural compatibility with silicate materials (cement, concrete), and has technical advantages in the field of cement reinforcement and concrete reinforcement. In addition, basalt fibers are a new type of green active, and environmentally friendly material with low cost, high performance, and ideal cleanliness [22]. Therefore, basalt fibers were used as the reinforcement material in the selection of fibers. Additionally, a suitable amount of basalt fiber was mixed to enhance the frictional properties of the soil. A small quantity of foaming agent (aluminum powder) was added to reduce the soil density without compromising its strength.

After conducting numerous orthogonal tests, considering the practical requirements of the project, foaming effects of the fiber-reinforced cured lightweight soil, and economic considerations, the final method for preparing the fiber-reinforced cured lightweight soil specimens was determined, as presented in Table 2.

The specimen preparation process is as follows:

(1) One end of a cylindrical glass tube with a 3.91 cm diameter and 8 cm height was sealed;

(2) The prepared fiber-reinforced cured lightweight soil was loaded into a glass tube and vibrated thoroughly to remove air voids. Controlled pressurized foaming was employed to regulate the foaming rate of the specimens. Once the mixture reached a specified height within the glass tube, the open end was sealed with a breathable impermeable cloth and a glass cap.

(3) The sealed specimen was placed on a flat surface and pressure was applied to the upper end of the glass tube using a heavy object to prevent foam expansion.

(4) After a maintenance period of 2-3 days, the specimens were demolded, wrapped in cling film, and placed in a controlled temperature and humidity chamber for further maintenance. The sample preparation is illustrated in Fig. 2. The age of the specimen is 28 days. After reaching the curing age, the specimens were subjected to basic physical property tests to obtain a table of basic physico-chemical properties, as shown in Table 3.

Test Methods

Wet and Dry Cycle Test Scheme

The aim of this study was to simulate the high rainfall and rapid evaporation conditions experienced during summer and study the effect of dry and wet cycles on fiber-reinforced cured lightweight soil specimens through tests. For the test preparation, the specimens were tightly wrapped in cling film and placed in a high and low temperature alternating damp heat apparatus maintained at 40ºC for dehumidification. The masses of the specimens were measured every 2 h, and when no significant changes were observed, the dehumidification process was considered complete. After dehumidification, the specimens were placed in a vacuum saturation tank for moisture absorption until a saturation level of 95% or higher was reached, indicating the completion of moisture absorption.

Based on preliminary tests, it was determined that dehumidification should be conducted for 15 h, followed by moisture absorption for 22 h to achieve complete dry-wet cycles.

The specimens were subjected to 0-15 wet and dry cycles, and the unconfined compressive strength was used to determine the optimal number of cycles. The variation curve of the unconfined compressive strength with the number of wet-dry cycles is presented in Fig. 3. As shown in Fig. 3, the unconfined compressive strength gradually stabilized after eight wet-dry cycles. Therefore, subsequent tests were conducted with 0, 1, 3, 5, and 8 wet-dry cycles.

Dynamic Triaxial Test Program

The tests were performed using a DDS-70 dynamic triaxial tester shown in Fig. 4. Considering the burial depth when using fiber-reinforced cured lightweight soil as the roadbed filler and poorly drained lower soil, the perimeter pressure was set to 25 kPa, and no drainage was allowed. The waveform employed was a sine wave resembling the traffic load at a frequency of 1 Hz. The magnitude of the dynamic stress was determined based on the results of the triaxial shear tests, and the cyclic stress ratio (CSR) was introduced as a damage

Table 2. Proportioning scheme for test materials.

Water content	Cement	Lime	Aluminum powder	Basalt fiber	Fiber length
100%	9%	2%	0.09	0.3%	15

Note: The percentages of cement, quicklime, aluminum powder, and basalt fiber are the percentages of the sum of the masses of soil and water.

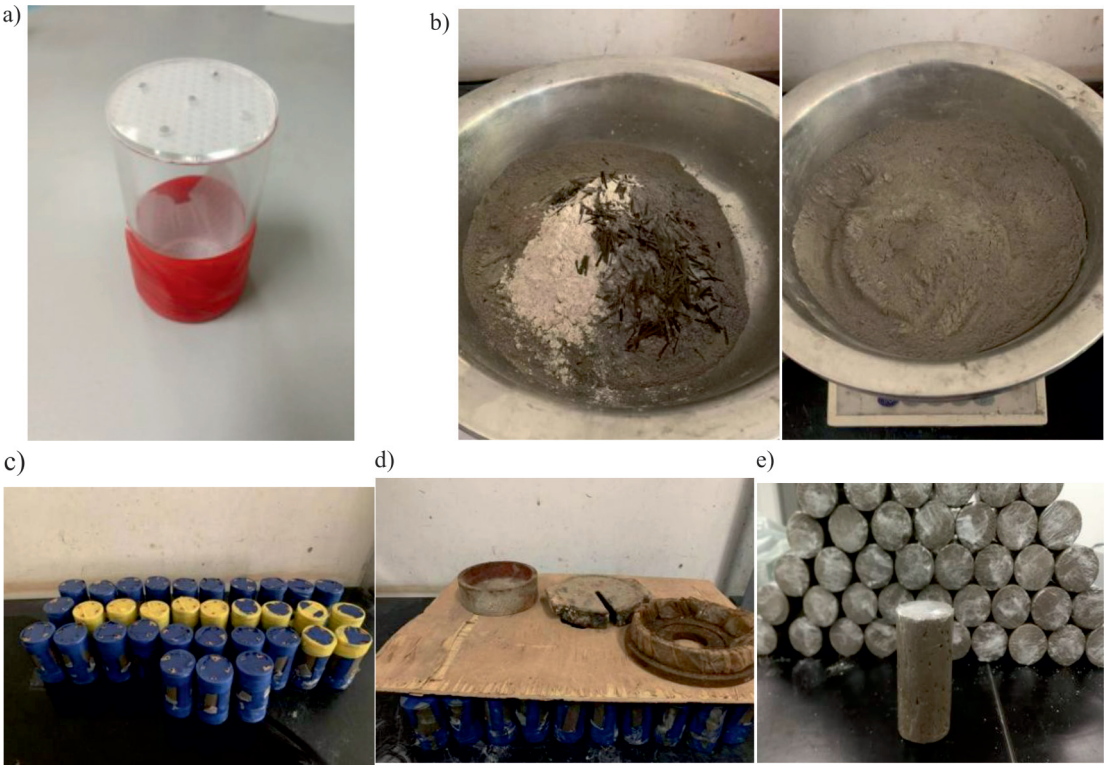

Fig. 2. Preparation process for sample: a) lolds, b) material mixing chart, c) assembly of the finished sample, d) pressing, e) finished specimen.

Table 3. Basic physical properties of cured soil.

Density ρ/ (g·cm^{-3})	Water content /%	28 days unconfined compressive strength /kPa
1.02	25.7	406

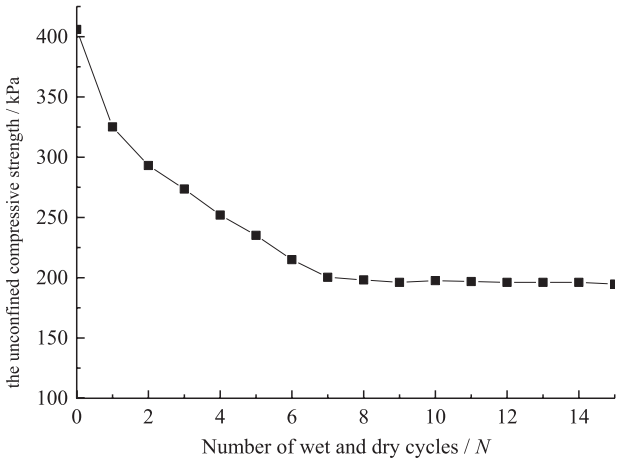

Fig. 3. Variations in unconfined compressive strength with the number of wet and dry cycles.

criterion when the strain reached 5%. Eq. (1) is used to calculate the CSR. By analyzing the Tianjin road traffic flow, the average hourly traffic flow on the expressway was computed, and the intermittent ratio (t) was set. Here, $t = t_1/t_2$, where t_1 is the stopping time, and t_2 is the loading time (t_2 = 10 s). The interval ratios were set to 0.5, 1, 3, and 10, respectively. The dynamic triaxial test program is presented in Table 4, and the loading program is presented in Table 5. A schematic of the loading schematic can be seen presented in Fig. 5.

$$CSR = \frac{\sigma_d}{2\sigma_3} \tag{1}$$

where CSR is the cyclic stress ratio, σ_3 is the surrounding pressure, and σ_d is the dynamic stress.

Test Results and Analysis

Accumulated Plastic Deformation

Based on the dynamic triaxial test results, we plotted and analyzed the cumulative dynamic strain curve of the fiber-reinforced cured lightweight soil under intermittent loading.

Single-Stage Intermittent Loading

Owing to space limitations, only selected figures are analyzed in this section. Fig.6 shows the cumulative plastic deformation curves of the fiber-reinforced cured lightweight soil under different numbers of wet and dry cycles at an intermittent ratio at t = 0.5. Fig. 7 presents

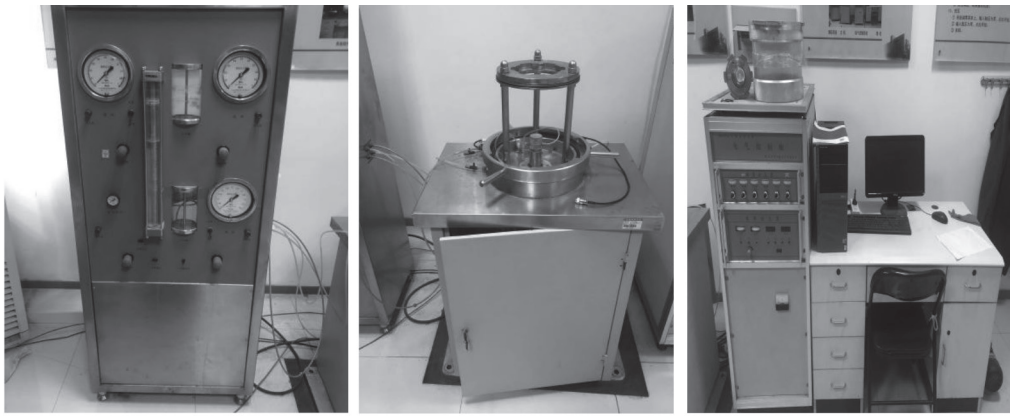

Fig. 4. DDS-70 strain-controlled dynamic triaxial tester. a) single-stage loading, b) Multi-stage loading.

Table 4. Dynamic triaxial test program.

Surrounding pressure /kPa	Dry-wet cycle/*N*	Wave form	Frequency /Hz	Intermittent ratio /t	Number of vibrations N_f	CSR
25	0, 1, 3, 5, 8	Sine wave	1	0.5, 1, 3, 10	30000	2, 3, 4, 5, 6, 7, 7.5

Note: Three parallel specimens were used for each group of tests, with an interval ratio $t = t_1/t_2$, where t_1 is the stopping time, and $t_2 = 10$ s is the loading time.

Table 5. Loading program.

Loading way	Intermittent ratio/*t*	Dry-wet cycle/*N*	CSR
Intermittent loading (Single-stage loading)	0.5, 1, 3, 10	0, 1, 3, 5, 8	2, 3, 4, 5, 6, 7, 7.5
Intermittent loading (Multi-stage loading)	0.5, 1, 3, 10	0, 1, 3, 5, 8	2, 3, 4, 5, 6, 7

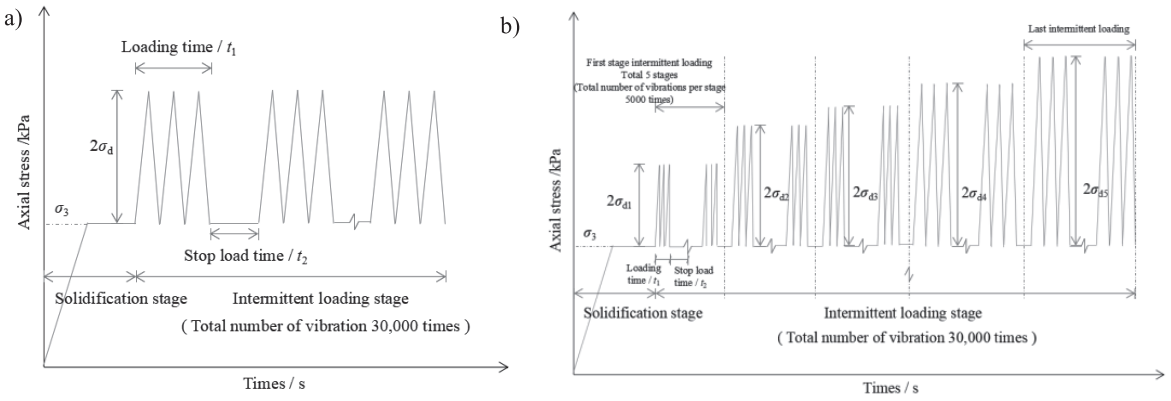

Fig. 5. Loading diagram: a) single-stage loading, b) multi-stage loading.

the cumulative plastic deformation curves under different intermittent ratios at N = 8 cycles.

Figs 6 and 7 show three forms of cumulative plastic deformation curves for the fiber-reinforced cured lightweight soils under single-stage intermittent loading: stable, critical, and destructive. For example, in Fig. 6e), when CSR = 2 and 3, the curve exhibits stable behavior. The accumulated plastic strain increases rapidly in the initial stage of loading and gradually stabilizes with an increasing number of vibration cycles (N_f), and the specimen reaches a stable state. When CSR = 5, the curve exhibits critical behavior. The accumulated plastic strain continues to increase with the increasing N_f, and although the strain growth rate decreases in the later stages of loading, it maintains a certain growth rate. If the loading continues, the specimen may get damaged by the excessive accumulated plastic strain. When CSR = 6 and CSR = 7, the curve represents stable damage. Under

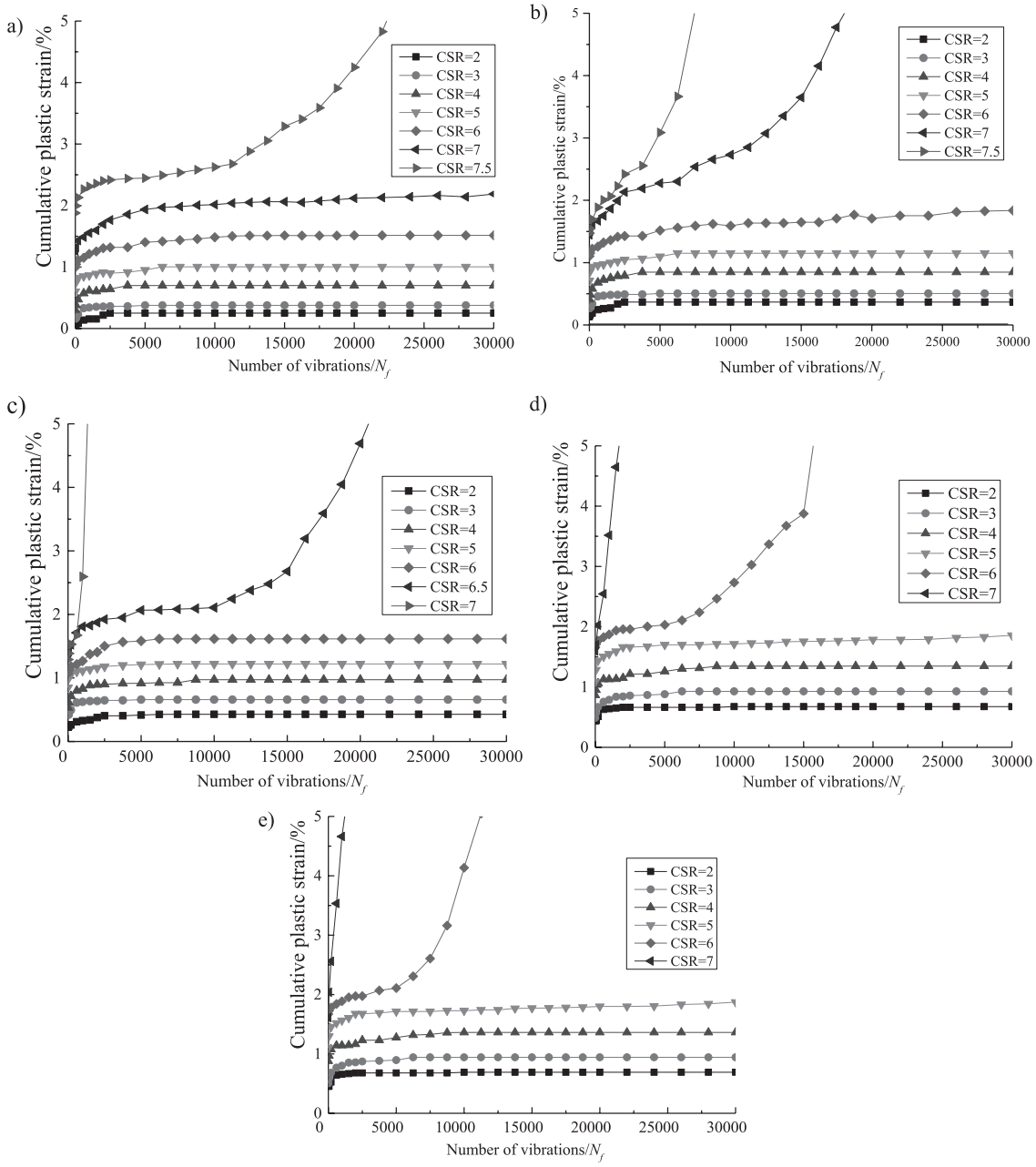

Fig. 6. Cumulative plastic deformation curve at t = 0.5. a) N = 0, b) N = 1, c) N = 3, d) N = 5, e) N = 8.

loading, the accumulated plastic strain of the specimen increases rapidly, and the soil undergoes damage.

The number of wet-dry cycles affected the accumulated plastic strain, as shown in Fig. 6. With an increase in the number of cycles, the accumulated plastic strain of the fiber-reinforced cured lightweight soil gradually increased and eventually stabilized. The first wet and dry cycles had the most significant effect, and after five cycles, the strain gradually decreased and stabilized around the eighth cycle. This behavior can be attributed to the strong structural properties of the fiber-reinforced cured lightweight soil, which exhibit strong cementation owing to the close arrangement of the particles. Consequently, soil that has not undergone wet-dry cycle processes undergo less deformation under external loads. After wet-dry cycles, the tiny pores of the cured soil were filled with water, causing the pores to gradually enlarge and even penetrate, resulting in reduced resistance to deformation in the soil. After eight cycles, the soil particle positions were adjusted to establish a new balance, leading to stabilized deformation.

Influence of Interval Duration

As illustrated in Fig. 7, the interval duration plays a significant role in influencing the plastic deformation behavior of the soil. Using CSR = 7 as an example, the cumulative plastic deformation curve at t = 0.5 indicates a destructive pattern, implying that the

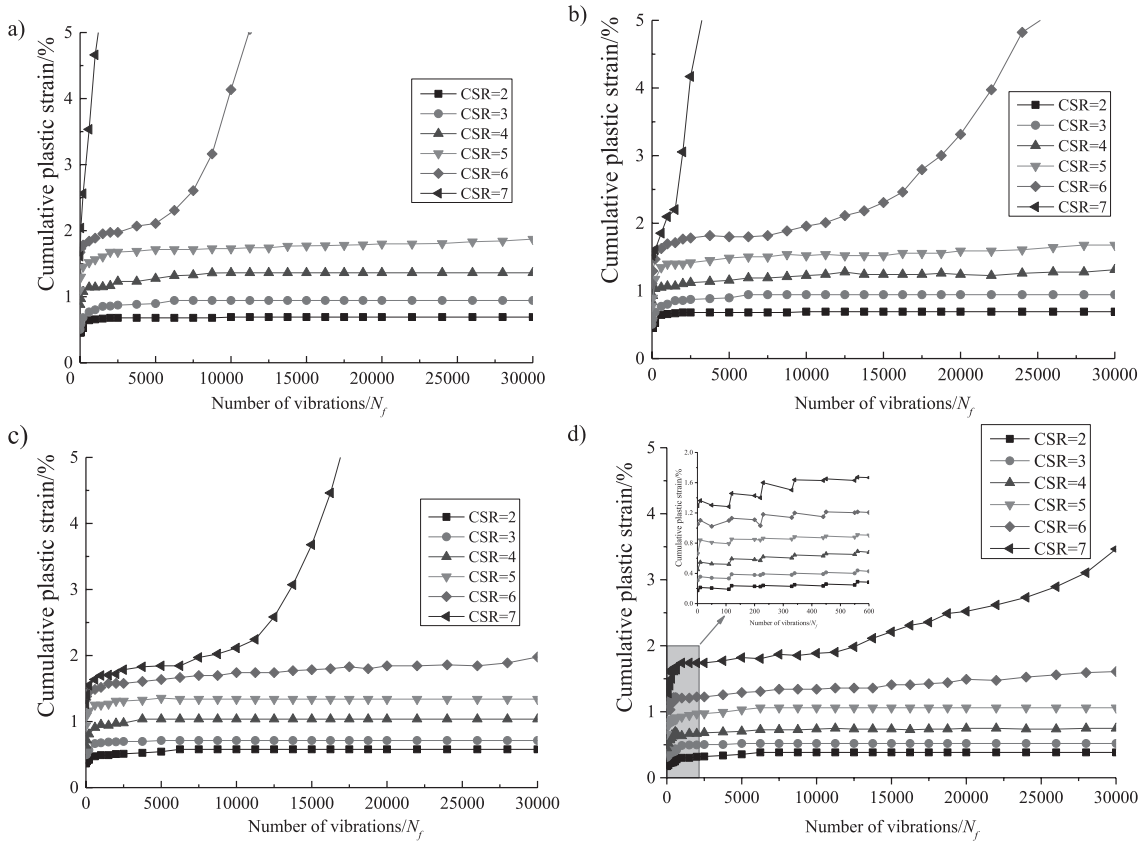

Fig. 7. Cumulative plastic deformation curve at N = 8. a) t = 0.5, b) t = 1, c) t = 3, d) t = 10.

specimen sustains damage even at smaller vibration cycles. In contrast, the cumulative plastic deformation curve at t = 10 displays a critical behavior, where the cumulative plastic strain rate increases but remains within the damage criterion.

This observation highlights that under continuous loading, the alignment and movement between soil particles lead to a more pronounced specimen deformation by rapidly pushing the soil body into the plastic creep stage. Conversely, intermittent loading allowed the soil to enter the plastic creep stage gradually and steadily throughout the loading process. This gradual progression enhances the ’resistance of the soil to deformation. Furthermore, excessive intervals enable the full recovery of the soil by reorganizing soil particles and redistributing stress, ultimately transforming the damaged specimen into a stable or critical state.

Multi-Stage Intermittent Loading

Based on the findings of single-stage intermittent loading, it can be inferred that the deformation of the specimen gradually stabilizes after undergoing eight dry-wet cycles. This indicates that the influence of the dry-wet cycles on the specimen reached its maximum effect. Consequently, fiber-reinforced cured lightweight soil, having undergone eight dry-wet cycles, was chosen for multistage intermittent loading, and its accumulated plastic deformation was analyzed; the results are illustrated in Fig. 8.

From the observations in Fig. 8, it can be noted that when the cyclic dynamic stress ratio is relatively small, the accumulated plastic strain of the specimen increases with an increase in the number of vibrations N_f and eventually stabilizes. Conversely, when the CSR is high, the accumulated plastic strain experiences rapid growth until it reaches the damage criterion defined during the test, thus marking the end of the test. For instance, considering t = 0.5, the specimen subjected to multi-stage intermittent loading undergoes a process of “recompression” at each stage. This indicates that the deformation increased rapidly during each stage and gradually stabilized, similar to the behavior observed during the initial loading. Finally, the specimen was damaged when the CSR reached 7.

The comparison between multi-stage and single-stage intermittent loading shows that the initial stage of cyclic stress in the multi-stage loading was relatively small and did not reach the structural yield stress of the specimen. As the number of vibrations increases, the specimens experience continuous compression, which enhances their ability to resist deformation. Consequently, at the same applied load, the accumulated plastic strain decreased, leading to a reduction in deformation. This agrees with the conclusions of Tang [23]. This also suggests that while the interval time can enhance the soil resistance to deformation and prevent

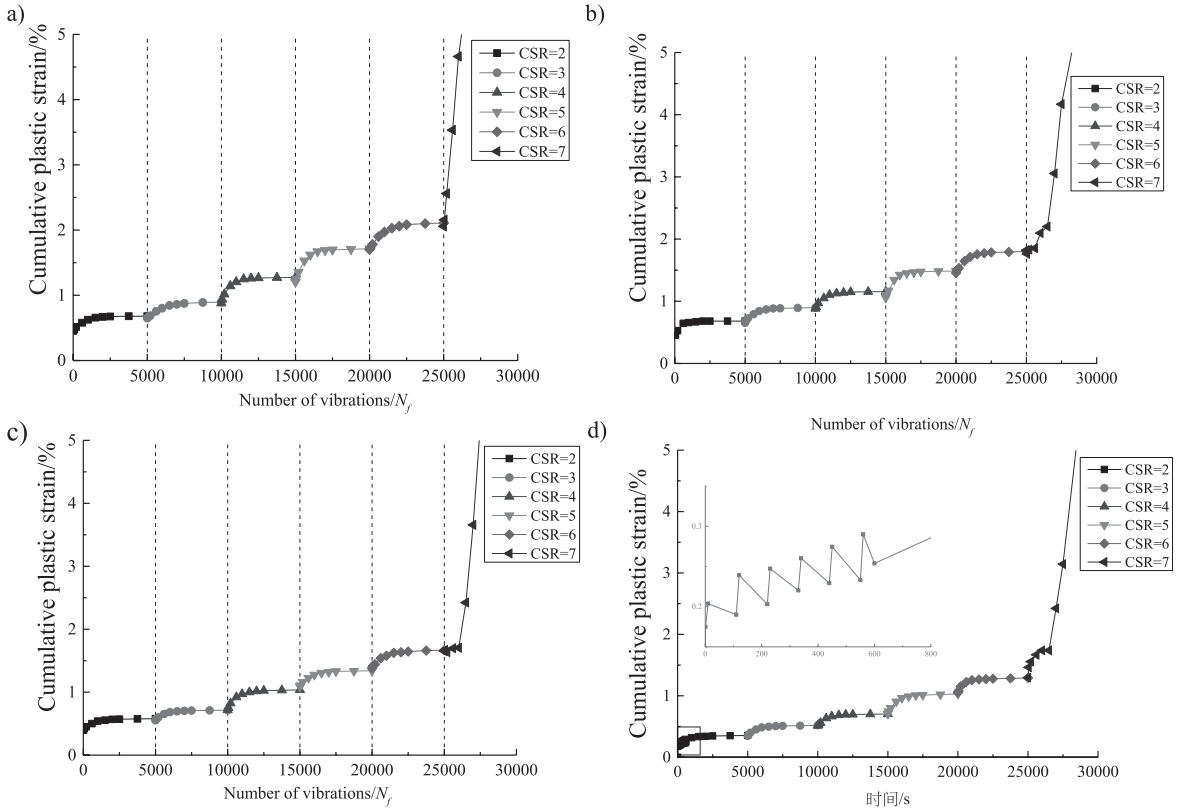

Fig. 8. Cumulative plastic deformation curve at N = 8. a) t = 0.5, b) t = 1, c) t = 3, d) t = 10.

the development of cumulative plastic deformation, the trend of cumulative plastic deformation during the late loading period is still determined by the magnitude of the cyclic dynamic stress ratio.

Accumulated Plastic Deformation Prediction

Predictive Model for Multi-Stage Intermittent Loading

The cumulative plastic deformation curve depicted in Fig. 8 provides valuable insights into the behavior of the fiber-reinforced cured lightweight soil under multistage intermittent loading. The cumulative plastic deformation curve under multistage intermittent loading differs significantly from that observed under single-stage intermittent loading. Therefore, it is crucial to predict the cumulative plastic strain of the fiber-reinforced cured lightweight soil accurately under multistage intermittent loading scenarios. Based on the observations made during single-stage intermittent loading, it is apparent that the influence of eight dry-wet cycles on soil deformation is considerable. Consequently, to assess different interval ratios, the most unfavorable dry-wet cycles (N = 8) were selected for analysis and prediction.

Given the prevalence of critical or stable states in roadbed soil in engineering practice, the ability to discern the damage-type curve based on the critical dynamic stress holds significant relevance [24]. Consequently, it is crucial to predict the changes in the cumulative plastic strain for soils that exhibit critical and stable behavior.

Conventional models employed for predicting the cumulative plastic deformation in soils include hyperbolic, exponential, and advection models, which consider multistage loading. Eqs (2)-(4) present the fundamental equations for the hyperbolic model [25], exponential model [26], and translational model considering multilevel loading [27], respectively.

$$\varepsilon_p = \frac{N_f}{a + bN_f} \tag{2}$$

$$\varepsilon_p = aN_f^{\,b} \tag{3}$$

$$\varepsilon_{1p}^{M+1} = \varepsilon_{1p}^{M} + \delta\varepsilon_{1p}^{M+1} \tag{4}$$

where: ε_p, $\varepsilon_{1p}{}^{M+1}$, $\varepsilon_{1p}{}^{M}$ are the accumulated plastic strains at different stages; parameters a, b, and δ are the correlation fitting parameters, and N_f is the vibration number.

These models provide valuable tools for estimating the cumulative plastic deformation and can aid in understanding the response of soils under various loading scenarios.

By enhancing the classical exponential model, an improved model was developed to predict the

accumulated plastic strain of specimens subjected to multistage intermittent loading.

Fig. 8 clearly illustrates this process. At each loading stage, the initial plastic strain was considered as the strain corresponding to the stress history. To further refine the analysis, equivalent vibrations were introduced. These vibrations represent the necessary vibrational input to attain the accumulated plastic strain at the conclusion of the preceding stage, under the specified load level at stage 'i' From Eqs (5)-(7), the accumulated plastic strain at stage *i* can be accurately computed.

$$\varepsilon_{pi} = a_i N_i^{b_i} \tag{5}$$

$$N_i^{:} = N - N_{i-1} + N_{i-1}^{eq} \tag{6}$$

$$N_{i-1}^{eq} = \left(\frac{\varepsilon_{pi-1}}{a_i} \right)^{\frac{1}{b_i}} \tag{7}$$

where ε_{pi} is the cumulative plastic strain at stage *i*, and N_{i-1}, ε_{pi-1} is the required number of vibrations and cumulative plastic strain at the end of stage *i*−1 loading; a_i and b_i are the fitting parameters for stage *i*.

These equations incorporate crucial elements for evaluating the cumulative plastic strain and enable a more comprehensive understanding of the response of the specimen to multistage intermittent loading.

In this study, an improved exponential model was implemented to obtain the fitting equation for the cumulative plastic deformation at each loading stage, along with the corresponding parameters. Eq. (8) is the derived fitting equation. Additionally, an analysis was conducted to explore the relationship between these parameters and the CSR. Subsequently, predictions were made for steady and critical cumulative plastic deformations under intermittent multistage loading.

Fig. 9 shows the fitting curves of the cumulative plastic strain at various loading levels, providing a visual representation of the accuracy of the model. Table 6 presents the specific values of the fitting parameters associated with each curve, offering a comprehensive reference for further analysis and comparison.

By employing the improved exponential model and considering the CSR, this study offers valuable insights into predicting and understanding the cumulative plastic deformation behavior under intermittent multistage loading.

$$\varepsilon_p = a - b \cdot c^{Nf} \tag{8}$$

Upon examining Table 6, it is evident that the values of parameter c exhibit minimal variation across different stress and intermittent ratios. Consequently, the mean value of parameter c = 0.9969 was adopted. The relationship equations between parameters a and b and the CSR are presented in Equations (9) and (10),

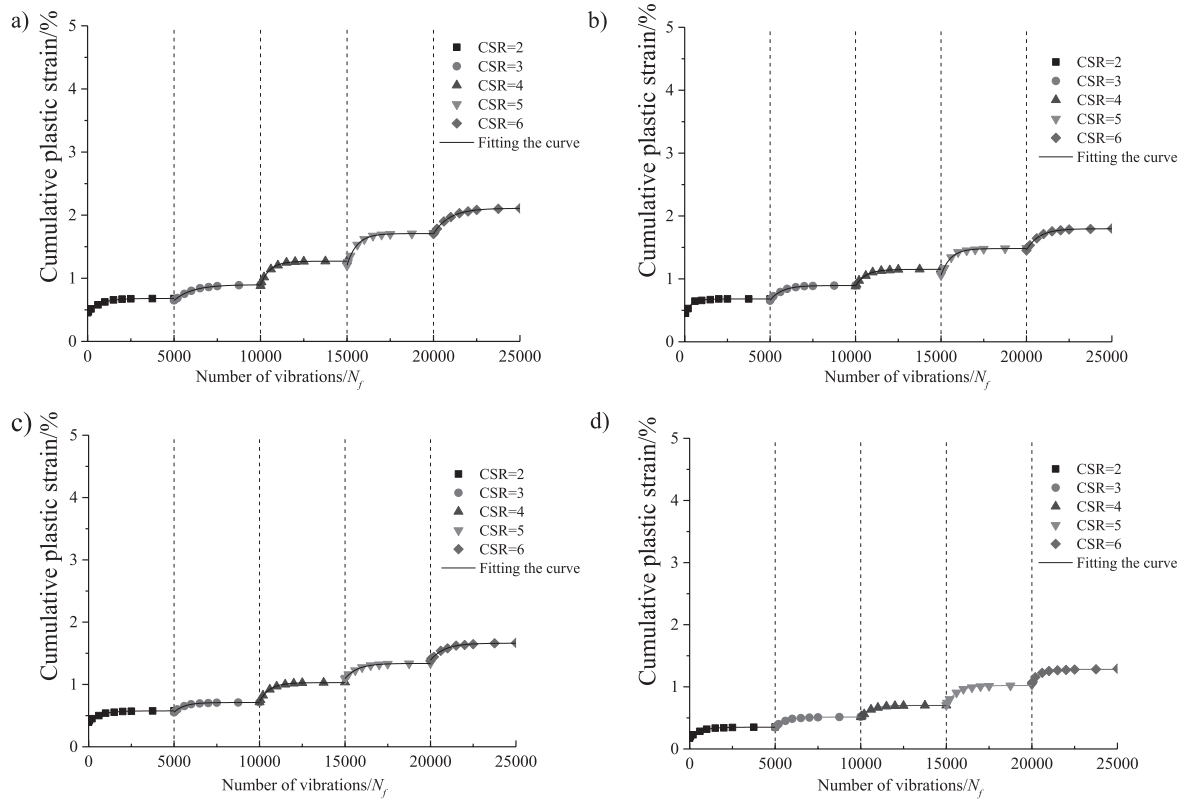

Fig. 9. Cumulative plastic strain fitting curve. a) t = 0.5, b) t = 1, c) t = 3, d) t = 10.

Table 6. Fitting parameter values.

Intermittent ratio	CSR	a	b	c	*c* Mean value	R^2
t = 0.5	2	0.68	0.22	0.99	0.9969	0.999
	3	0.89	28.7	0.99		0.998
	4	1.27049	3.8044	0.99816		0.99683
	5	1.708	1.012	0.998		0.999
	6	2.1085	1.1060	0.9989		0.9998
t = 1	2	0.68068	0.23932	0.99747		0.98715
	3	0.8948	337.82	0.9985		0.9968
	4	1.152	4.9364	0.9983		0.99735
	5	1.482	2.629	0.998		0.997
	6	1.79795	1.9323	0.9986		0.997
t = 3	2	0.57611	0.17497	0.99851		0.99635
	3	0.7105	628.144	0.99834		0.9987
	4	1.0292	8.2297	0.9982		0.997
	5	1.3376	2.06423	0.99863		0.9974
	6	1.6625	1.8580	0.9987		0.995
t = 10	2	0.35	0.167	0.998		0.99361
	3	0.513	812.1	0.988		0.9972
	4	0.7007	2.7584	0.9983		0.9985
	5	1.021	1.455	0.998		0.997
	6	1.28094	1.08437	0.99774		0.99093

Table 7. Fitting values for parameters *a*, *b* and *c* on the cyclic stress ratio.

Parameter		*t* = 0.5	*t* = 1	*t* = 3	*t* = 10
a	*n*	0.2689	0.3225	0.233	0.1249
	m	1.1444	0.9497	1.0884	1.2949
	R^2	0.9875	0.9878	0.98709	0.9884
b	b_0	1.77933	1.6002	1.36566	0.90207
	l	3.27975	3.26774	3.26276	3.20067
	o	0.23261	0.22439	0.22924	0.22188
	p	105.84338	685.14937	1208.95303	1221.10013
	R^2	0.99683	0.99987	0.99997	0.99999
c	0.9969				

respectively. The corresponding fitted parameter values are listed in Table 7.

$$a = n \cdot CSR^m \tag{9}$$

$$b = b_0 + l \cdot e^{\left[-0.5\times\left(\frac{CSR-o}{p}\right)^2\right]} \tag{10}$$

Analyzing Table 7 and summarizing each parameter in *a* and *b*, the following equations are obtained, see Eqs (11)-(16).

$$n = -0.018t + 0.3024,\ R^2 = 0.8902 \tag{11}$$

$$m = 0.0315t + 0.9801,\ R^2 = 0.8998 \tag{12}$$

$$b_0 = -0.0843t + 1.7174 \text{, } R^2 = 0.9481 \quad (13)$$

$$l = -0.008t + 3.2818 \text{, } R^2 = 0.9824 \quad (14)$$

$$o = -0.0011t + 0.2326 \text{, } R^2 = 0.9912 \quad (15)$$

$$p = 1228.8 - 2334.1 \times 0.2318^t \text{, } R^2 = 0.999 \quad (16)$$

The specific formulas for a and b are given in Eqs (17) and (18), respectively.

$$a=(-0.018t+0.3024)\cdot CSR^{(0.0314t+0.9801)} \quad (17)$$

$$b = (-0.0843t + 1.7174) + (-0.008t + 3.2818) \times e^{-0.5\times\left(\frac{CSR+0.0011t-0.2326}{1228.8-2334.1\times0.2318^t}\right)^2} \quad (18)$$

Eqs (5)-(7) can be interpreted as representing a single-stage intermittent loading scenario in which the entire vibration process consists of only one stage. Therefore, Equation (5) can also be used to estimate the cumulative plastic strain of lightly consolidated soils such as river and lake bottom mud under single-stage intermittent loading conditions.

Validation of Cumulative Plastic Strain Model

To validate the accuracy of the cumulative plastic strain equation for fiber-reinforced cured lightweight soil under intermittent loading, the test results and the fitted values obtained from the equation were compared.

The fiber-reinforced cured lightweight soil specimens were prepared according to the material mix ratios listed in Table 2. After a maintenance period of 28 days, the specimens underwent eight cycles of wetting and drying. Subsequently, a dynamic triaxial test was conducted with an interval ratio of t = 5 while keeping the other test parameters constant. The deformation curves were then plotted and juxtaposed with the simulation results for detailed analysis. The specific findings are shown in Fig. 10.

From the observations shown in Fig. 10, it is evident that the fitted values of the cumulative plastic strain align well with the experimental results. This successful alignment indicates that Equation (5) can be effectively employed to forecast the deformation progression of fiber-reinforced cured lightweight soils under intermittent loading conditions.

The satisfactory agreement between the predicted values and actual test outcomes substantiates the accuracy and reliability of the proposed equation. This validation provides valuable insights into the deformation behavior of fiber-reinforced cured lightweight soil and contributes to the understanding and prediction of its performance in real-world geotechnical engineering applications.

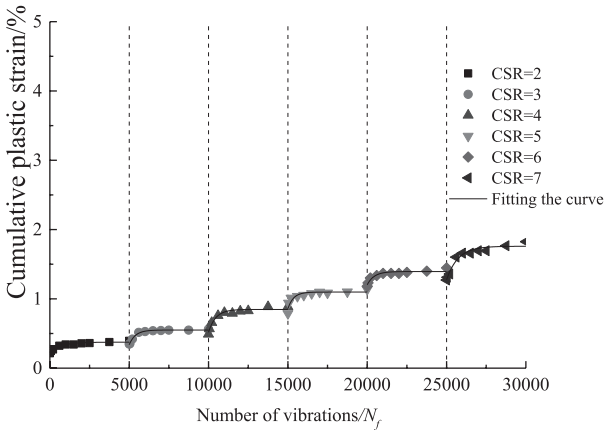

Fig. 10. Verification of cumulative deformation curve.

Conclusion

To comprehensively analyze the deformation characteristics of fiber-reinforced cured lightweight soil under the influence of dry-wet cycles and intermittent loading, a series of dynamic triaxial tests were conducted. The tests were aimed at investigating the impact of the number of dry-wet cycles, intermittent ratio, and cyclic stress ratio on the accumulated plastic deformation of the soil. Based on the test results, a prediction model was proposed to assess the soil behavior under intermittent loading conditions. The key conclusions drawn from this study are as follows.

The accumulated plastic deformation of the fiber-reinforced cured lightweight soil gradually increased and eventually stabilized as the number of wet–dry cycles increased. Notably, the initial wet-dry cycles had the most significant effect on deformation, and the strain exhibited a tendency to decrease and stabilize after approximately five cycles, reaching a relatively steady state after approximately eight cycles.

2. The interval duration plays a crucial role in controlling the accumulated plastic deformation of soil. The interval duration effectively enhanced the resistance of the soil to deformation by allowing the full recovery of elastic deformation during the interval stage. In the multistage intermittent loading tests, the development of the accumulated plastic deformation was primarily influenced by the magnitude of the cyclic dynamic stress ratio.

3. By refining the existing exponential model, an improved exponential model was developed to predict the accumulated plastic strain resulting from intermittent loading, encompassing both single-stage and multistage loading scenarios. The model exhibited favorable prediction accuracy, reinforcing its utility for predicting roadbed deformation under lower traffic conditions.

Acknowledgments

The authors wish to acknowledge the support of the National Natural Science Foundation of China (Grant Nos. 5197844, 42177119, 42377141), the Tianjin Science and Technology Plan Project (Grant No. 19JCZDJC39700).

Conflict of Interest

The authors declare no conflict of interest.

References

1. POONI J., ROBERTT D., GIUSTOZZI F., SETUNGE S., XIE Y.M., XIA J.J.T.G. Performance evaluation of calcium sulfoaluminate as an alternative stabilizer for treatment of weaker subgrades. Transportation Geotechnics. **27**, 100462, **2021**.
2. LIU H., ZHAO J., WANG Y., YI N., CUI C. Strength Performance and microstructure of Calcium Sulfoaluminate Cement -stabilized Soft Soil. Sustainability. **13** (4), 2295, **2021**.
3. SUN R.J., FANG C., GAO F. L., GE Z., ZHANG H. Z., LU Q. Study on pavement performance and solidified mechanism of solidified soil based on solid waste. China Journal of Highway and Transport. **34** (10), 216, **2021**.
4. CHEN X.R., BAI Y.B.L.G. Evaluation study on the benefits of solidification of sediment in urban rivers and lakes. Journal of China Institute of Water Resources and Hydropower Research. **13** (1), 54, **2015**.
5. YE W.J., WU Y.T., YANG G.S., JING H., CHANG S., CHEN M. Study on microstructure and macro-mechanical properties of paleosol under dry-wet cycles. Chinese Journal of Rock Mechanics and Engineering. **38** (10), 2126, **2019**.
6. LI J.D., TANG C.S., ZENG H., SHI B. Evolution of desiccation cracking behavior of clays under drying-wetting cycles. Rock and Soil Mechanics. **42** (10), 2763, **2021**.
7. CHEN R., ZHANG X., HAO R.Y., BAO W.X. Shear strength deterioration of geopolymer stabilized loess under wet-dry cycles: mechanisms and prediction model. Rock and Soil Mechanics. **43** (05), 1164, **2022**.
8. FANG J.J., XUE T.X., YANG X.L., YU J.X., ZHANG J., FENG Y.X. Soil water characteristics of expansive soil considering the effects of drying and wetting cycles and volume change under dehydration Path. China Journal Rock Mechnical Engineering. **41** (08), 1671, **2021**
9. ZHANG Z.L., WU S.R., TANG H.M., WANG T., XING P. Dynamic characteristics and microcosmic damage effect of loess and mudstone. Chinese Journal of Rock Mechanics and Engineering. **36** (5), 1256, **2017**.
10. LIU Z.Q., WANG B., WANG F., ZHANG Y.C. Dynamic characteristics of the underlying soil of subway tunnel under cyclic loading. China Civil Engineering Journal. **53** (S1), 194, **2020**.
11. RAO P.S., LI D., MENG Q.S., FU J.X., LEI X.W. Study on earth pressure distribution characteristics of calcareous sand foundation under cyclic loading. Rock and Soil Mechanics. **42** (06), 1579, **2021**.
12. LONG A.F., CHEN K.S. Experimental study on dynamic characteristics of red clay under wet-dry cycles. Journal of Guangxi University (Natural Science). **44** (1), 122, **2019**.
13. LIU S.Z., HE Z.M., YANG Y. Experimental study on dynamic characteristics of coarse-grained soil under dry-wet cycle and load. Highway & Motor Transport. **6**, 66, **2018**.
14. CHEN L.Q., CHEN J.H., ZHANG J.S. Dynamic properties of cement improved argillite-slate coarse-grained siol under drying-wetting cycles. Journal of Hunan University (Natural Science). **44** (9), 107, **2017**.
15. CHEN Y., ZHAO Q., CHAN D. Impact and predictio of wetting-drying on seismic response of silty clay. Journay of China Gorges University (Natural Sciences). **39** (6), 52, **2017**.
16. WANG T.H., HAO Y.Z., WANG C., CHENG L., LI J.L. Experimental study on dynamic strenth propertise of compacted losee under wetting-drying cycles. Chinese Journal of Rock Mechanics and Engineering. **39** (6), 1242, **2020**.
17. ZHONG X.M., WANG Q., LIU Z.Z., BAI L., MA J., LIU F., WANG J. Dynamic strength of fly ash-modified loess subgrade under influences of drying-wetting cycle. Chinese Journal of Geotechnical Engineering. **42** (S1), 95, **2020**.
18. FUJIWARA H., UE S. Effect of preloading on post -construction consolidation settlement of soft clay subjected to repeated loading. Soils and Foundations -Tokyo-. **30** (1), 76, **2008**.
19. ZHENG Q.Q., XIA T.D., ZHANG M.Y., ZHOU F. Strain prediction model of undisturbed silty soft clay under intermittent cyclic loading. Journal of Zhejiang University (Engineering Science). **54** (5), 889, **2020**.
20. ZHENG Q.Q., XIA T.D., ZHANG M.Y. Stiffness degradation of soft clay under cyclic loading considering intermittency effect. Journal of Haerbin Institute of Technology. **52** (11), 88, **2022**.
21. NIE R.S., LI Y.F., LENG W.M., MEI H.H., DONG J.L., CHEN X.X. Deformation characteristics of fine-grained soil under cyclic loading with intermittence. Acta Geotechnica. **15** (11), 3041, **2020**.
22. LI J., YANG L., HE L., GUO R. W., LI X. Y., CHEN Y. C., MUHAMMAD Y., LIU Y. Research progresses of fibers in asphalt and cement materials: a review. Journal of Road Engineering. **3** (1), 35, **2023**.
23. TANG L., YAN M.H., LING X.Z., TIAN S. Dynamic behaviours of railway's base course materials subjected to long-term low-level cyclic loading: experimental study and empirical model. Geotechnique. **67** (6), 537, **2017**.
24. HEATH D.L., WATERS J.M., SHENTON M.J., SPARROW R.W. Design of conventionalrail track foundation. Proceedings of the Institution of Civil Engineers. **51** (2), 251, **1972**.
25. ZHU Y.H., LIU G.B., XIE Q.F., ZHENG R.Q. Accumulative plastic strain model of soft clay considering temperature effect and its verification. China Earthquake Engineering. **41** (4), 901, 961, **2019**.
26. MONISMITH C.L., OGAWA N., FREEME C.R. Permanent deformation characteristics of subgrade soils due to repeated loading. Transport Research Record. **537**, 1, **1975**.
27. WANG H.L., CUI Y.J., LAMAS-LOPEZ F., DUPLA J.C., CANOU J., CALON N., CHEN R.P. Permanent deformation of track-bed materials at various inclusion contents under large number of loading cycles. Journal of Geotechnical and Geoenvironmental Engineering. **144** (8), 04018044, **2018**.